Ultrasound stimulation of piezoelectric nanocomposite hydrogels boosts cartilage regeneration

Leonardo Ricotti (leonardo.ricotti@santannapisa.it)
Scuola Superiore Sant'Anna
Andrea Cafarelli
Scuola Superiore Sant'Anna
Cristina Manferdini
IRCCS Istituto Ortopedico Rizzoli
Diego Trucco
Scuola Superiore Sant'Anna
Lorenzo Vannozzi
Scuola Superiore Sant'Anna
Elena Gabusi
IRCCS Istituto Ortopedico Rizzoli
Francesco Fontana
Scuola Superiore Sant'Anna
Paolo Dolzani
IRCCS Istituto Ortopedico Rizzoli
Yasmin Saleh
IRCCS Istituto Ortopedico Rizzoli
Enrico Lenzi
IRCCS Istituto Ortopedico Rizzoli
Marta Columbaro
IRCCS Istituto Ortopedico Rizzoli
Manuela Piazzi
Consiglio Nazionale delle Ricerche
Jessika Bertacchini
University of Modena and Reggio Emilia
Andrea Aliperta
Scuola Superiore Sant'Anna
Markys Cain
National Physacal Laboratory https://orcid.org/0000-0002-8413-3104
mauro gemmi

https://orcid.org/0000-0001-9542-3783
Paola Parlanti
Istituto Italiano di Tecnologia
Carsten Jost
PlasmaChem GmbH
Yirij Fedutik
PlasmaChem GmbH
Gilbert Nessim
Bar-Ilan University
Madina Telkhozhayeva
Bar-Ilan University
Eti Teblum
Bar-Ilan University
Erik Dumont
Image Guided Therapy
Chiara Delbaldo
IRCCS Istituto Ortopedico Rizzoli
Giorgia Codispoti
IRCCS Istituto Ortopedico Rizzoli
Lucia Martini
IRCCS Istituto Ortopedico Rizzoli
Matilde Tschon
IRCCS Istituto Ortopedico Rizzoli
Milena Fini
IRCCS Istituto Ortopedico Rizzoli
Gina Lisignoli
IRCCS Istituto Ortopedico Rizzoli

Physical Sciences - Article

Keywords:

Posted Date: November 30th, 2022

DOI: https://doi.org/10.21203/rs.3.rs-2326785/v1

Abstract

Osteoarthritis implies a progressive degeneration of the whole joint. Cartilage is particularly affected, with inflammation playing a pivotal role1. In recent years, cartilage regeneration has been pursued through several bioengineering strategies and using different stem cell types2-6. Adipose -derived mesenchymal stromal cells (ASCs) constitute an intriguing and minimally invasive option. However, the use of ASCs for cartilage regeneration is hampered by a relatively inefficient expression of key chondrogenic markers7. Thus, new strategies to boost both in situ targeting and chondrogenesis of ASCs are highly desirable. Here we show that ASCs embedded in a nanocomposite hydrogel including piezoelectric nanomaterials and graphene oxide nanoflakes, and stimulated with ultrasound waves with precisely controlled parameters (1 MHz and 250 mW/cm2, for 5 min once every two days for a period of 10 days) dramatically boost cell chondrogenic commitment. Furthermore, this stimulation regimen also has a considerable anti-inflammatory effect. The proposed nanocomposite hydrogel also shows excellent biocompatibility in vivo. Our results show for the first time the chondrogenic potential of the combined piezoelectric nanoparticle-ultrasound stimulus; the proposed paradigm has the potential to trigger cartilage regeneration in osteoarthritis, focal cartilage defects and other pathological conditions involving cartilage lesions and degeneration. Future efforts should expand preclinical data, and target clinical applications of this therapeutic strategy.

Main Text

Osteoarthritis (OA) is one of the most common causes of pain and disability in middle-aged and elderly people[8]. Progressive cartilage degeneration is the hallmark of such pathology, with a central role of inflammation in this process[1]. Different bioengineering approaches and stem cell types have been explored in the last decades to target cartilage regeneration, with interesting results, especially in recent years[2-6]. In this endeavor, adipose -derived mesenchymal stromal cells (ASCs) are a particularly attractive option since they can be harvested from the patient with a relatively simple, safe, and minimally invasive procedure (*i.e.*, liposuction). ASCs recently demonstrated potential for OA treatment, evidencing an anti-inflammatory paracrine action and the ability to favor homeostasis recovery in the OA cartilage[9,10].

However, there is limited evidence of clinical benefits, due to ASC difficulties in engrafting and reconstituting the deteriorated cartilage tissue effectively[7,11]. New strategies to boost both *in situ* targeting and chondrogenesis of ASCs are thus needed, since they would considerably enhance the efficacy of these cells in OA treatment. Despite some exciting efforts in this direction[12-16], sustained expression of the key chondrogenic markers (*e.g.*, type II collagen, aggrecan, glycosaminoglycans) and the consequent formation of a mature articular cartilage tissue remains hard to accomplish at present.

We hypothesized that nanocomposite hydrogels embedding graphene oxide (GO) nanoflakes and piezoelectric barium titanate nanoparticles (BTNPs), stimulated with dose-controlled ultrasound (US) waves, boost the chondrogenic differentiation of ASCs laden in the scaffold (**Fig. 1a**, **Supplementary video 1**).

Nanocomposite cell-laden hydrogel

The hydrogel used in this work was based on a two-components bioinstructive matrix (RGD-VitroGel®) doped with GO nanoflakes and BTNPs.

Firstly, we assessed the chemical-physical features of BTNPs (**Fig. 1b,c**, **Extended Data Fig. 1a-c**) and of BTNPs coated with propylene glycol alginate (PGA), to enhance their stability in aqueous solution (**Extended data Fig. 1d-f**). These nanoparticles showed no cytotoxicity on human chondrocytes, even at high concentrations, up to 100 µg/mL (**Extended data Fig. 1g-j**). Then, we assessed the chemical-physical features of GO nanoflakes (**Fig. 1d**) and GO nanoflakes coated with polydopamine (PDA) (**Extended data Fig. 2a-c**). These nanomaterials showed excellent safety on human chondrocytes up to 25 µg/mL (**Extended data Fig. 2d-g**). A more detailed discussion on BTNPs and GO nanoflake characterization results can be found in **Supplementary information, section S1**.

Based on these results and hints derived from the state-of-the-art[17-21], we selected 25 µg/mL as GO nanoflake concentration and 50 µg/mL as BTNP concentration to build the nanocomposite hydrogel (named "Nanocomp"), in which two million ASCs/mL were embedded (**Extended data Fig. 3a**). As shown in **Fig. 1e**, after two days of culture, the GO nanoflakes remained confined outside the cells, whereas BTNPs tended to be internalized and accumulated in intracellular vacuoles.

The non-doped hydrogel (named "Hydrogel") and the Nanocomp showed no relevant difference in their FT-IR spectra (**Extended data Fig. 3b**) and rheometric properties (**Extended data Fig. 3c**). Consistent with previous reports[22,23] (although focused on different nanomaterial types) we found that the addition of the nanofillers produced an increase of the compressive modulus, and a decrease of the swelling ratio and the sol fraction (**Extended data Fig. 3d-f**). The Nanocomp consistency index (K) and flow behavior index (n) (**Fig. 1f,g**) allowed estimating the shear stress acting on cells during material injection (see Methods), for different needle sizes: 18, 20, 22, and 24 G diameters (**Fig. 1h**). Shear stress values reached up to ~ 35 Pa, a value that is well below the critical threshold of 5 kPa[24] that may hamper cell viability during the extrusion. The nanocomposite mass considerably decreased after 60 days and the hydrogels entirely dissolved after three months (**Extended data Fig. 3g**). Although the RGD-VitroGel® was featured by chemical groups similar to the ones of alginate, its degradation properties resulted rather different[25]. The coefficient of friction (COF) was in the range featuring the human cartilage (0.001-0.35)[26] (**Extended data Fig. 3h**), without any evident sign of wear (variation of COF over time)[27]. We found that the force needed to inject the nanocomposite in its pre-crosslinked status was smaller than 10 N, a value considered suitable for the injection of materials for *in vivo* applications (EN ISO 7886-1:2018), for the needle sizes of 22, 20 and 18 G, whereas it resulted larger for 24G (**Extended data Fig. 3i**). In view of an *in situ* delivery of this material on the cartilage surface, we also verified that the nanocomposite stably remained on the cartilage surface at any angle, except at 90° (**Extended data Fig. 3j**); furthermore, the mechanical stress needed to detach the material from the cartilage was higher than 10 kPa, considered a clinically acceptable threshold[28] (**Fig. 1i**). Interestingly, we found that GO nanoflakes play a crucial role in

enhancing adhesion, while BTNPs did not show any relevant concentration-dependent effects (**Extended data Fig. 3k,l**), This result seems in contradiction with previous reports, claiming that smaller particles enable larger adhesion forces[29]. This is probably due to the flake-like shape of GO, which resulted more effective than spherical BTNPs, in promoting adhesion.

Stimulation of nanocomposite hydrogel through dose-controlled ultrasound waves

To activate the piezoelectric nanoparticles and create local electrical inputs, we stimulated the Nanocomp with US waves using a set-up that allowed precise control of the dose delivered to materials and cells and the exploration of a broad range of frequencies (38 kHz – 5 MHz) and intensities (0 – 1000 mW/cm^2) (**Fig. 2a,b**, **Extended data Fig. 4a**, **Supplementary videos 2,3**). Previous reports in which piezoelectric nanomaterials were stimulated with US waves, adopted US sources and set-ups[20,30-33] that did not guarantee reliable control of the dose at the target[34]. However, this aspect is crucial to precisely know the amount of energy corresponding to the desired biological effects and to facilitate future clinical translation[35].

Modeling the interaction between US waves and piezoelectric nanomaterials is another important, but under-explored aspect. An analytical model of a single nanoparticle invested by US was developed by Marino and colleagues[20]. For the same purpose, finite element model (FEM) simulations have also been recently proposed[30,32,33]. We developed a new simplified analytical model based on Gauss's law (**Supplementary information, section S2**), finding that the voltage generated (V) can be expressed as:

$$V = \frac{R \cdot d_h \cdot P_{US}}{\epsilon_r \cdot \epsilon_0} \qquad (2)$$

where R is the nanoparticle radius, d_h is the piezoelectric hydrostatic coefficient (related to the more usually observed d_{33}, or d_{31}/d_{32} coefficients of barium titanate), P_{US} is the ultrasound pressure amplitude, ε_R and ε_0 are the dielectric constants of the material (relative dielectric constant) and of the free space, respectively (**Fig. 2c**).

Then, a FEM model was implemented (see Methods). First, the single particle was modeled, showing that individual BTNPs yielded a piezoelectric charge proportional to the applied hydrostatic pressure, exhibiting a good correspondence between the analytical model and the FEM simulations (**Fig. 2d,e**). Afterward, the entire cell-laden nanocomposite was modeled. For this purpose, a series of transmission electron microscopy (TEM) images showing the relative positions and distances of cells, BTNPs and GO nanoflakes in the system were acquired, and data extracted as reported in **Supplementary information, section S3**. This allowed creating a set of BTNP clusters, representative of particle density and distribution within the cell. Finally, a FEM model of the entire nanocomposite was developed (**Fig. 2f**). Results showed that larger nanoparticle clusters generated greater electrical fields when excited by the US wave. We found that the voltage reached values up to 43.1 μV when a peak-to-peak pressure ($P_{pk\text{-}pk}$) of

172 kPa was applied (corresponding to 250 mW/cm^2, found as the optimal stimulation intensity, as described below). Interestingly, the electric field streamlines spread into the cell cytoplasm well beyond the diameter of the single nanoparticle cluster (**Fig. 2g**, **Extended data Fig. 4b**, **Supplementary video 4**). To the best of our knowledge, this is the first time a model estimates the voltage generated in a cell, based on the experimental distribution of nanoparticles and their clusters within the cell cytoplasm, also evaluating the streamline distribution in the cell cytoplasm.

Viability and chondrogenic commitment of ASCs in the nanocomposite hydrogel

The viability of ASCs embedded in the Nanocomp for up to 7 days resulted in a high percentage of viable cells on days 2 and 7 (**Fig. 3a**), associated with a significant decrease in the rate of cytotoxicity on day 7 (**Fig. 3b**).

As a first US stimulation regime, we considered a frequency of 1 MHz, an intensity of 250 mW/cm^2, a pulsed repetition frequency of 1 kHz, a 20% duty cycle and a stimulation time of 5 min. This choice emerged from considerations derived from the state-of-the-art: although the dose-controlled US stimulation of piezoelectric nanocomposites is still unexplored, it is known that the above-mentioned parameters fit the typical low-intensity pulsed ultrasound (LIPUS) regime widely used for *in vitro* and *in vivo* applications[36] and also the safety limits of physiotherapy domain[37]. We applied the ultrasonic stimulation to samples once every 2 days for an overall duration of 10 days.

Four experimental groups (Hydrogel or nanocomposite with or without US) were considered (**Extended data Fig. 5a**). We first checked if the presence of such a stimulus raised undesired effects on the cells. Results highlighted on day 10 a homogeneous cell distribution (**Extended data Fig. 5b**) and high cell viability (**Extended data Fig. 5c**), showing no negative effects induced by the nanoparticles or the US stimulus. Cytotoxicity analyses showed even an LDH reduction mainly in “Nanocomp + US" samples (**Extended data Fig. 5d**), whereas the metabolic activity was not modulated (**Extended data Fig. 5e**). Finally, the evaluation of senescent and apoptotic cells confirmed the same percentage of positive cells from day 2 to day 10 in both – US and +US samples (**Extended data Fig. 5f,g**).

Results on day 10 also showed an evident overexpression of cartilage-related markers *COL2A1* and *ACAN* (**Fig. 3c**) in the “Nanocomp + US”, compared to the other groups. Furthermore, the transcription factor *SOX9*, the proliferating gene *MKI67* and the fibrotic gene *COL1A1* were significantly downregulated in “nanocomp +US”, whereas the *COL10A1* hypertrophic gene was not modulated (**Extended data Fig. 5h**). Immunohistochemical analyses of collagen type 2 and proteoglycans confirmed a marked increase of these cartilage-related protein markers in the “Nanocomp + US” compared to the other groups, on day 10 (**Fig. 3d**). Interestingly, on day 10, US stimulation in the nanocomposite reduced ECM degradation by inducing *TIMP1* anabolic factor by decreasing the *MMP13/TIMP1* ratio (**Extended data Fig. 5i**).

Then, we assessed the biological response of ASCs laden in a nanocomposite hydrogel embedding 12.5 µg/mL of GO nanoflakes and 25 µg/mL of BTNPs (half of the concentrations previously used). Results highlighted that such a reduced concentration of nanomaterials produced a much less evident

chondrogenic effect on cells, both at gene and protein levels, on day 10 (**Extended data Fig. 6a,b**). We also verified the impact of a prolonged US stimulation on the samples: we performed an additional experiment in which we applied US stimulation to samples once every 2 days, for an overall duration of 10 days, and then leaving the samples in culture until day 28 ("priming" group, similar to the one reported above). In parallel, we analyzed the behavior of a "control" group, in which US stimulation was not provided, and the one of a "chronic" group, in which US stimulation was continued once every 2 days for the whole period of 28 days (**Extended data Fig. 6c**). We found that chondrogenic markers were more expressed in the priming group with respect to the control one and to the chronic one, on day 28 (**Extended data Fig. 6d**). Furthermore, the chronic group showed overexpression of collagen type 1, which is undesirable when cartilage regeneration is targeted[38] (**Extended data Fig. 6e**). These results highlight that an excessive US stimulation has adverse effects on chondrogenic markers and promotes the expression of fibrotic ones. This finding is in agreement with previous evidences[39], although obtained on bone marrow-derived mesenchymal stem cells laden in a 3D agarose matrix, without the addition of any nanomaterial, and using cyclic hydrostatic pressure instead of US waves.

Finding the optimal US dose and exploring the underlying mechanisms

The dose-controlled US stimulation set-up described above (**Fig. 2a,b**) allowed exploring other stimulation regimes in a controlled way. This enabled us to find the optimal US dose guaranteeing a boost in the chondrogenesis. First, we varied the US frequency, adding to 1 MHz (previously investigated) also 38 kHz and 5 MHz (**Extended data Fig. 7a**). Results showed that 38 kHz could not be used for this purpose, since such a frequency produced mechanical damages to the hydrogel (**Extended data Fig. 7b**), probably due to an excessive mechanical index (that is maximized at low frequencies). US-induced modifications of the polymer structures at low frequencies are often exploited for promoting drug delivery[40,41]. However, in our case, the interference with the crosslinked hydrogel matrix hampered the construct integrity. Comparing the results obtained with 1 MHz and 5 MHz applied to the Nanocomp, we found that, on day 10, 1 MHz was more efficient than 5 MHz in inducing the expression of the chondrogenic genes *COL2A1* and *ACAN*, without affecting the proliferating gene *MKI67* and keeping the *SOX9* gene higher (**Fig. 3e**). Collagen type 2 immunostaining on day 28 confirmed the positive effect of 1 MHz compared to 5 MHz (**Fig. 3f**). Both US frequencies did not affect the cell cytotoxicity rate and metabolic activity (**Extended data Figure 7c,d**).

Then, we kept the frequency fixed at 1 MHz and we varied the US intensity, adding to 250 mW/cm^2 (previously investigated) also 125 and 500 mW/cm^2 (**Extended data Fig. 7e**). Results showed that on day 10, the intensity of 250 mW/cm^2 was more efficient than 125 and 500 mW/cm^2 in inducing the expression of *COL2A1* and *ACAN* genes, without modulating the proliferative gene *MKI67* and still keeping the *SOX9* gene higher (**Fig. 3g**). Immunohistochemical analyses on day 28 of collagen type 2 confirmed that 250 mW/cm^2 was the most efficient intensity to induce chondrogenesis (**Fig. 3h**). Cytotoxicity and metabolic activity were not affected by such stimulation regime (**Extended data Fig. 7f,g**). Once the optimal US dose was identified, TEM imaging performed on day 28 on the "Nanocomp + US" samples revealed the presence of both single cells with a round morphology or associated to form a

chondron-like structure and collagen fibers showing the typical banding characteristics of collagen type 2, confirming the positive chondrogenic effects of this stimulation regime (**Fig. 3i**). These results show for the first time the chondrogenic potential of the combined piezoelectric nanoparticle + US stimulus. In fact, previous reports highlighted the possible benefits of this paradigm on bone differentiation[42,43], but never on cartilage differentiation. Furthermore, this is the first example in which different US parameters (frequency and intensities) were screened, by carefully controlling the dose of energy delivered, and finding the optimal one for triggering the BTNP-mediated biological effects.

We explored more in-depth the mechanisms responsible for the ASC response to the generated piezopotential. First, we performed a proteomic analysis, comparing the nanocomposite without US stimuli (as a control) and the nanocomposite stimulated with US, on day 10 of differentiation. A total of 960 proteins were identified for “Nanocomp – US” and 604 for “Nanocomp + US”. Among those proteins, 572 were common to both datasets, as illustrated in the Venn diagram (**Fig. 4a)**, of which 32 resulted differentially regulated in the “Nanocomp + US” sample. Gene ontology analysis showed that US stimulation influenced biological processes involved in mechano-transduction, such as cytoskeleton and extracellular matrix organization, collagen fibril organization and collagen metabolic processes. Cell adhesion and cell migration processes were also enriched. Notably, signaling pathways such as non-canonical Wnt, regulating the cytoskeleton, and integrin-mediated signaling pathway, were enriched in US-stimulated samples (**Fig. 4b**, **Extended data Fig. 8a,b**). Additional details are reported in **Supplementary information, section S4**.

Then, we designed an experiment as depicted in **Extended data Fig. 8c**, using the Nanocomp and simulating the OA inflammatory environment by using the typical catabolic cytokine IL1β, with and without US (named “Infl + US” and “Infl – US”, respectively), compared to the counterparts exposed to a physiological environment (“Norm + US” and “Norm – US”). Results highlighted that the inflammatory milieu induced the release of IL6 and IL8 on day 2 (**Fig.4c**). The US treatment significantly down-modulated both cytokines already on day 3 (after one US stimulation); this effect was even more evident on day 10 (after five US stimulations) (**Fig. 4d,e**). Interestingly, on day 10, when the US treatment considerably reduced the inflammatory cytokines, bringing them to levels close to a normal condition, we evidenced an increase of the *COL2A1* cartilage-specific gene (**Fig. 4f**). On day 28, we confirmed the presence of areas positive to collagen type 2 (**Fig. 4g**). These results highlight that the specific US stimulation regime used, in combination with the nanocomposite, exerted a dual effect: it was efficient in inhibiting inflammatory cytokines and, at the same time, in boosting ASC chondrogenesis.

In vitro genotoxicity and *in vivo* biocompatibility assays

In vitro genotoxicity and *in vivo* safety assessments for the Nanocomp were conducted according to ISO 10993-1 (2018) standards, by assuming the Nanocomp as an implant medical device in long-term contact (> 30 days) with the target tissue.

The procedure and results of the Ames test with and without metabolic activation are reported in **Extended data Fig. 9a-b** and in the **Supplementary information, section S5**. Neither the six tested concentrations of the Nanocomp nor the non-disgregated one exhibited mutagenicity: concentration-response trend and fold increase in revertant colonies over the baseline greater than 2.0 were not found in any strain with and without metabolic activation. The micronuclei test (**Extended data Fig. 9c**) demonstrated that none of the three tested concentrations of the Nanocomp (0.75X, 1X and 1.25X) caused an increase in cytotoxicity. No statistically significant increases were found in micronuclei frequencies compared to the negative control after short- and long-term exposure to the test substance, whereas positive controls always induced significant increases (**Fig. 4g**, **Extended data Fig. 9d** and **Supplementary information, section S6**). Overall, these results indicate that the nanocomposite hydrogel did not induce chromosomal damages on TK6 cells under the experimental conditions.

In vivo skin irritation tests performed in rabbits (**Extended data Fig. 10a**) showed no skin reactions (oedema or erythema) in all sites treated with the Nanocomp at any observation time after material removal. Primary Irritation Index (PII) values are reported in **Fig. 4h** and **Supplementary information, section S7**. The irritation response for the Nanocomp can be considered negligible. Acute systemic toxicity tests were performed in rats (**Extended data Fig. 10b**). No signs of toxicity were found in the animals treated with the Nanocomp, with no significant decrease in body weight, daily water and food consumption in comparison with the control group (**Fig. 4i**). No clinical alterations in the main systems and apparatuses were recorded.

Finally, delayed-type hypersensitivity tests were performed on guinea pigs (**Extended data Fig. 10c**). Results are shown in **Fig. 4j**: 48 h after material removal, none of the animals in the Nanocomp and negative control groups showed erythema or oedema, indicators of cellular-mediated hypersensitivity reactions, or any other skin reactions, whereas 7 guinea pigs out of 10 treated with a known sensitizer had patchy and confluent erythema. The sensitization rate was 0% in the Nanocomp and negative control groups, and 70% in the positive control group. According to the classification criteria by Magnusson and Kligman based on the sensitization rate, Nanocomp and negative control resulted weak, whereas positive control resulted a strong sensitizer.

Conclusions

Although promising, the use of ASCs for cartilage regeneration is hampered by a relatively insufficient expression of key chondrogenic markers. Our findings show that ASCs embedded in a nanocomposite hydrogel including piezoelectric nanomaterials and graphene oxide nanoflakes and stimulated with US at 1 MHz and 250 mW/cm^2, dramatically boost their chondrogenic commitment *in vitro*, already on day 10. The nanocomposite hydrogel also shows excellent biocompatibility *in vivo.* Furthermore, the optimal US stimulation parameters found to trigger the nanocomposite also show a considerable anti-inflammatory effect. This is relevant, being inflammation a hallmark of OA onset and progression[1]. Overall, these results suggest that the nanocomposite material and the US stimulation regime used in this work can be

used to trigger cartilage regeneration in OA and other pathological conditions involving cartilage lesions and degeneration.

Main References

1. Liu-Bryan, R. & Terkeltaub, R. Emerging regulators of the inflammatory process in osteoarthritis. *Nat. Rev. Rheumatol.* **11**, 35-44 (2015).
2. Gaharwar, A.K., Singh, I., & Khademhosseini, A. Engineered biomaterials for in situ tissue regeneration. *Nat. Rev. Mater.* **5**, 686-705 (2020).
3. Murphy, M.P. et al. Articular cartilage regeneration by activated skeletal stem cells. *Nat. Med.* **26**, 1583-1592 (2020).
4. Sun, Y., You, Y., Jiang, W., Wang, B., Wu, Q., & Dai K. 3D bioprinting dual-factor releasing and gradient-structured constructs ready to implant for anisotropic cartilage regeneration. *Sci. Adv*. **6**, eaay1422 (2020).
5. Huang, J. et al. 3D printed gelatin/hydroxyapatite scaffolds for stem cell chondrogenic differentiation and articular cartilage repair. *Biomater. Sci.* **9**, 2620-2630 (2021).
6. Wei, W., & Dai, H. Articular cartilage and osteochondral tissue engineering techniques: Recent advances and challenges. *Bioact. Mater.* **6**, 4830-4855 (2021).
7. Martin, I., Galipeau, J., Kessler, C., Le Blanc, K. & Dazzi, F. Challenges for mesenchymal stromal cell therapies. *Sci. Transl. Med.* **11**, eaat2189 (2019).
8. Cui, A., Li, H., Wang, D., Zhong, J., Chen, Y., & Lu, H. Global, regional prevalence, incidence and risk factors of knee osteoarthritis in population-based studies. *EClinicalMedicine* **29**, 100587 (2020).
9. Pers, Y.M. et al. ADIPOA Consortium. Adipose mesenchymal stromal cell-based therapy for severe osteoarthritis of the knee: a phase I dose-escalation trial. *Stem Cells Transl. Med.* **5**, 847-856 (2016).
10. Lee, W.S., Kim, H.J., Kim, K.I., Kim, G.B., & Jin, W. Intra-articular injection of autologous adipose tissue-derived mesenchymal stem cells for the treatment of knee osteoarthritis: a phase IIb, randomized, placebo-controlled clinical trial. *Stem Cells Transl. Med.* **8**, 504-511 (2019).
11. Zha, K. et al. Heterogeneity of mesenchymal stem cells in cartilage regeneration: from characterization to application. *NPJ Regen. Med.* **6**, 1-15 (2021).
12. Go, G. et al. Human adipose-derived mesenchymal stem cell-based medical microrobot system for knee cartilage regeneration in vivo. *Sci. Robot*. **5**, eaay6626 (2020).
13. Zhou, M. et al. Graphene oxide: a growth factor delivery carrier to enhance chondrogenic differentiation of human mesenchymal stem cells in 3D hydrogels. *Acta Biomater.* **96**, 271-280 (2019).
14. Zhao, H., Liu, M., Zhang, Y., Yin, J., & Pei, R. Nanocomposite hydrogels for tissue engineering applications. *Nanoscale* **12**, 14976-14995 (2020).
15. Ghanbari, M., Salavati-Niasari, M., & Mohandes, F. Thermosensitive alginate-gelatin–nitrogen-doped carbon dots scaffolds as potential injectable hydrogels for cartilage tissue engineering applications.

RSC Adv. **11**, 18423-18431 (2021).

16. Pardo, A., Gómez-Florit, M., Barbosa, S., Taboada, P., Domingues, R.M., & Gomes, M.E. Magnetic nanocomposite hydrogels for tissue engineering: design concepts and remote actuation strategies to control cell fate. *ACS Nano* **15**, 175-209 (2021).
17. Paci, C. et al. Piezoelectric nanocomposite bioink and ultrasound stimulation modulate early skeletal myogenesis. *Biomater. Sci.* **10**, 5265-5283 (2022).
18. Vannozzi, L. et al. Graphene oxide and reduced graphene oxide nanoflakes coated with glycol chitosan, propylene glycol alginate, and polydopamine: characterization and cytotoxicity in human chondrocytes. *Nanomaterials* **11**, 2105 (2021).
19. Dubey, A.K., Thrivikraman, G., & Basu, B. Absence of systemic toxicity in mouse model towards $BaTiO_3$ nanoparticulate based eluate treatment. *J. Mater. Sci. Mater. Med.* **26**, 1-11 (2015).
20. Marino, A. et al. Piezoelectric nanoparticle-assisted wireless neuronal stimulation. *ACS Nano* **9**, 7678-7689 (2015).
21. Ciofani, G. et al. Effects of barium titanate nanoparticles on proliferation and differentiation of rat mesenchymal stem cells. *Coll. Surf. B: Biointerf.* **102**, 312-320 (2013).
22. Zaragoza, J., Fukuoka, S., Kraus, M., Thomin, J., & Asuri, P. Exploring the role of nanoparticles in enhancing mechanical properties of hydrogel nanocomposites. *Nanomaterials* **8**, 882 (2018).
23. Zaragoza, J. et al. Experimental investigation of mechanical and thermal properties of silica nanoparticle-reinforced poly (acrylamide) nanocomposite hydrogels. *PLoS One* **10**, e0136293 (2015).
24. Blaeser, A., Duarte Campos, D.F., Puster, U., Richtering, W., Stevens, M.M., & Fischer, H. Controlling shear stress in 3D bioprinting is a key factor to balance printing resolution and stem cell integrity. *Adv. Healthc. Mater.* **5**, 326-333 (2016).
25. Barceló, X., Eichholz, K.F., Garcia, O., & Kelly, D.J. Tuning the degradation rate of alginate-based bioinks for bioprinting functional cartilage tissue. *Biomedicines* **10**, 1621 (2022).
26. O'Connell, G., Garcia, J., & Amir, J. 3D bioprinting: new directions in articular cartilage tissue engineering. *ACS Biomater. Sci. Eng.* **3**, 2657-2668 (2017).
27. Trucco, D. et al. Graphene oxide-doped gellan gum-PEGDA bilayered hydrogel mimicking the mechanical and lubrication properties of articular cartilage. *Adv. Healthc. Mater.* **10**, 2001434 (2021).
28. Wang, D.A. et al. Multifunctional chondroitin sulphate for cartilage tissue–biomaterial integration. *Nat. Mater.* **6**, 385-392 (2007).
29. Arno, M.C. et al. Exploiting the role of nanoparticle shape in enhancing hydrogel adhesive and mechanical properties. *Nat. Commun.* **11**, 1-9 (2020).
30. Ma, B. et al. Piezoelectric nylon-11 nanoparticles with ultrasound assistance for high-efficiency promotion of stem cell osteogenic differentiation. *J. Mater. Chem. B* **7**, 1847-1854 (2019).
31. Zhao, D. et al. Electromagnetized nanoparticle-modulated neural plasticity and recovery of degenerative dopaminergic neurons in the mid-brain. *Adv. Mater.* **32**, 2003800 (2020).

32. Zhu, P., Chen, Y., & Shi, J. Piezocatalytic tumor therapy by ultrasound-triggered and $BaTiO_3$-mediated piezoelectricity. *Adv. Mater.* **32**, 2001976 (2020).
33. Li, C. et al. Wireless electrical stimulation at the nanoscale interface induces tumor vascular normalization. *Bioact. Mater.* **18**, 399-408 (2022).
34. Snehota, M., Vachutka, J., Ter Haar, G., Dolezal, L., & Kolarova, H. Therapeutic ultrasound experiments in vitro: review of factors influencing outcomes and reproducibility. *Ultrasonics* **107**, 106167 (2020).
35. Cafarelli, A. et al. Piezoelectric nanomaterials activated by ultrasound: the pathway from discovery to future clinical adoption. *ACS Nano* **15**, 11066–11086 (2021).
36. Jiang, X. et al. A review of low-intensity pulsed ultrasound for therapeutic applications. *IEEE Trans. Biomed. Eng.* **66**, 2704-2718 (2018).
37. EN 60601-2-5:2015, *Medical electrical equipment.* Part 2-5: *Particular requirements for the basic safety and essential performance of ultrasonic physiotherapy equipment* (2015).
38. Tschaikowsky, M. et al. The articular cartilage surface is impaired by a loss of thick collagen fibers and formation of type I collagen in early osteoarthritis. *Acta Biomater.* **146**, 274-283 (2022).
39. Puetzer, J., Williams, J., Gillies, A., Bernacki, S., & Loboa, E.G. The effects of cyclic hydrostatic pressure on chondrogenesis and viability of human adipose-and bone marrow-derived mesenchymal stem cells in three-dimensional agarose constructs. *Tissue Eng. Part A* **19**, 299-306 (2013).
40. Salgarella, A.R. et al. Investigation of drug release modulation from poly (2-oxazoline) micelles through ultrasound. *Sci. Rep.* **8**, 1-13 (2018).
41. Wei, P., Cornel, E.J., & Du, J. Ultrasound-responsive polymer-based drug delivery systems. *Drug Deliv. Transl. Res.* **11**, 1323-1339 (2021).
42. Kaliannagounder, V.K. et al. Remotely controlled self-powering electrical stimulators for osteogenic differentiation using bone inspired bioactive piezoelectric whitlockite nanoparticles. *Nano Energy* **85**, 105901 (2021).
43. Heng, B.C., Bai, Y., Li, X., Meng, Y., Zhang, X., & Deng, X. Signaling pathways implicated in enhanced stem/progenitor cell differentiation on electroactive scaffolds. *Smart Mater. Med.* **3**, 4-11 (2022).

Methods

Nanomaterial synthesis

BTNPs were synthesized by hydrothermal synthesis. Briefly, titanium hydroxide precursors were washed with CO_2-free, deionized water. Then, the gels were suspended together with $Ba(OH)_2 \cdot 8\ H_2O$ in a 1,4-butanediol/water mixture (1:2). The resulting suspension was placed in a 700 mL Teflon container within a stainless-steel pressure vessel. The reaction vessel was then heated at a rate of 5 °C/min to 220 °C and kept for 48 h. The resulting powders were washed with pH-adjusted (pH = 10) CO_2-free deionized water to remove the unreacted barium present in the solution and to prevent the incongruent dissolution of barium ions from the $BaTiO_3$ particle surface. GO nanoflakes were synthesized as previously reported[1]. BTNPs

and GO were autoclaved through vapor steam (30 min at 121 °C) to ensure their sterilization, according to ISO standard 17665-1:2006.

Nanomaterial characterization

The size of BTNPs was estimated by the BET method (Brunauer–Emmett–Teller theory) using a Belsorp-mini II (Belsorp) based on the curves of adsorption/desorption of N_2 by the nanoparticle powder. The specific surface area (SSA) was calculated, and the particle diameter was determined as follows:

$$d = \frac{6000}{SSA * \rho}$$

where ρ= 6.02 g/cm^3 is the density of $BaTiO_3$.

The size and morphology of the BTNPs were also analyzed through Transmission Electron Microscopy (TEM). A drop of autoclaved BTNPs in water suspension (100 µg/mL) was deposited onto a 300-mesh carbon-coated copper grid (TedPella). TEM analysis was carried out using a Libra 120 Plus microscope (Carl Zeiss, Oberkochen, Germany) operating at an accelerating voltage of 120 keV, equipped with an in-column omega filter for energy-filtered imaging, and with a bottom-mounted 12 bit 2k × 2k CCD camera (TRS).

The piezoelectric properties of autoclaved BTNPs were investigated through piezoelectric force microscopy (PFM), performed using an Icon Bruker AFM system (Dimension Icon, Bruker Co., USA), in the Peak Force PFM modality. A silicon probe (DDESP-V2, Bruker, Billerica, MA, USA), with a measured spring constant of 132.5 N/m, a resonant frequency of 486 kHz, and a deflection sensitivity of 57.4 nm/V was used. The amplitude of the piezoelectric signal and the hysteresis (sample bias from -10 to 10 V), were acquired in the vertical direction via lock-in detection by applying to the tip an alternating current voltage (V_{ac}) of 2 V at 300 kHz, outside the tip resonance frequency. Five independent samples were analyzed with a scan frequency of 0.25 Hz, and the average value of the d_{33} piezoelectric coefficient was calculated as follows:

$$d_{33} = A/V_{ac}$$

where A is the amplitude signal (pm). A reference sample made of polyvinyl fluoride (PVDF) in the form of a thin film (Goodfellow, thickness: 28 µm, d_{33}: ~ -20 pC/N) was also analyzed to properly calibrate the PFM amplitude signal.

Atomic force microscopy (AFM) measurements were carried out on GO nanoflakes, deposited on Si/SiO_2 wafers, using a Bio FastScan scanning probe microscope (Bruker, Dimension Icon & FastScan Bio, Karlsruhe, Germany). All images were obtained using PeakForce Quantitative Nanomechanical Mapping

mode with a Fast Scan C (Bruker) silicon probe (spring constant: 0.45 N/m). The images were captured in the retrace direction with a scan rate of 1.5 Hz. The resolution of the images was 512 samples/line.

Nanomaterial coating

A PGA (degree of esterification < 80%, Carbosynth, Staad, St. Gallen, Switzerland) solution was prepared at a concentration of 2.5 mg/mL in deionized water and then filtrated (filter size: 0.22 µm) at room temperature (RT). The autoclaved BTNPs were added in a ratio of 1:1 w/w to the polymeric solutions. Then, a sonication process with an ultrasound probe (power: 25 W, time: 30 min, frequency: 20 kHz, Bandelin SonoPuls HD4050, Berlin, Germany) allowed enhancing the interaction between the polymer and the BTNPs, favoring nanomaterial dispersion in aqueous media.

The coating of GO nanoflakes with PDA was performed as follows: autoclaved GO (5 mg/mL) was suspended in an aqueous solution made of dopamine hydrochloride (Sigma-Aldrich) at a concentration of 5 mg/mL in deionized water, previously filtered (filter size: 0.22 µm, material: PES) and adjusted in terms of pH by drop addition of 1 M NaOH solution (Sigma-Aldrich) to achieve a value of 8.5. The solution was sonicated with an ultrasound probe (power: 25 W, time: 300 s, frequency: 20 kHz). Finally, the mixture was stirred vigorously for 24 h at room temperature in the dark.

Dynamic light scattering (DLS) and zeta potential measurements were performed using a Zetasizer NanoZS90 (Malvern Instruments Ltd., Worcestershire, UK), analyzing the average size and polydispersity index (PDI) immediately after sonication and 3 and 7 days from the nanomaterial preparation. The samples were dispersed in deionized water and cell culture medium (Chondrocyte Growth Medium without phenol red, Cell Inc. Application), setting the concentration for all sample types to 100 µg/mL. Six independent samples were analyzed for each sample type.

X-ray photoelectron spectroscopy (XPS) analysis was carried out to verify the coating presence on the BTNPs and GO nanoflakes. XPS was performed using a Nexsa spectrometer (Thermo Scientific, Sunnyvale, USA) equipped with a monochromatic, micro-focused, low-power Al Ka X-ray source (photon energy: 1486.6 eV). High-resolution spectra were acquired at a pass energy of 50 eV. The source power was 72 W. The measurements were carried out under ultra-high-vacuum conditions, at a base pressure of 5×10^{-10} torr (not higher than 3×10^{-9} torr). The spectra obtained were analyzed and deconvoluted using the Vision software (Kratos). Overlapping signals were analyzed after deconvolution into Gaussian/Lorentzian-shaped components.

Assessment of nanomaterial cytotoxicity on human chondrocytes

The nanomaterial cytotoxicity was preliminarily evaluated on human articular chondrocytes (Cell Applications Inc., Boston, MA, USA), by carrying out Live/Dead assay, DNA quantification, metabolic activity analysis and LDH release quantification. The detailed protocols used for these tests are described in **Supplementary information, section S8.1**.

Nanocomposite hydrogel preparation

VitroGel RGD® was purchased from Well Bioscience (North Brunswick, NJ, USA) and prepared following the manufacturer's protocol. Briefly, the VG-RGD solution was mixed at RT with the Dilution Solution Type 1® (The Well Bioscience, North Brunswick, NJ, USA) at the ratio 1:2 up to obtain a uniform mixture. Then, Dulbecco Modified Eagle Medium (DMEM) (Life Technologies, Bleiswijk, The Netherlands) with a suspension of ASCs to reach the final cell density into the hydrogel of 2×10^6 cells/mL was added at the ratio of 4:1 (pre-crosslinked solution: DMEM with cells) at RT and mixed. Hydrogels doped with GO nanoflakes and BTNPs (referred as nanocomposite) were obtained following the same procedure but adding the nanomaterials at concentrations of 25 µg/mL and 50 µg/mL, respectively, and mixing at RT until obtaining a uniform solution. Finally, 300 µL of both cell-laden non-doped or nanocomposite mixtures were gently transferred into a cell crown (Scaffdex, Finland), and inserted into a 24-wells plate. After 20 min of stabilization at RT, further 150 µL of DMEM were placed over the hydrogel for 1 h to allow saturation of the ionic crosslinking. Finally, 1.5 mL of DMEM were added to each well and the samples incubated at 37 °C and 5% CO_2.

TEM imaging of the nanocomposite hydrogel

For ultrastructural evaluation, the hydrogels were fixed with 2.5% glutaraldehyde in 0.1 M cacodylate buffer (pH = 7.4) for 1 h at RT and for 3 h at 4°C. Afterward, samples were postfixed with 1% osmium tetroxide in 0.1 M cacodylate buffer for 2 h at 4°C, dehydrated in an ethanol series, infiltrated with propylene oxide and embedded in Epon resin. Cross-sections of each hydrogel were cut to allow internal analysis. Ultrathin sections (80 nm-thick) were stained with uranyl acetate and lead citrate (15 min each) and observed with a Jeol Jem 1011 transmission electron microscope (Jeol Jem, USA), operated at 100 kV. Images were captured using an Olympus digital camera and iTEM software. Unstained ultrathin sections were observed with a Zeiss Libra 120 plus TEM operating at 120 keV, and equipped with a Bruker XFlash 6T-60 SDD detector for Energy Dispersive X-ray spectroscopy (EDX).

Chemical-physical characterization of the nanocomposite hydrogel

The chemical features of the sample were characterized through Fourier Transform Infrared Spectroscopy (FT-IR) and by Nuclear Magnetic Resonance (NMR) spectra recording. The physical features were assessed by rheometry (which also allowed estimating the shear stresses acting on the cells during injection), uniaxial compression tests, tribological measurements, and degradation tests in different media. The detailed protocols are described in **Supplementary information, section S8.2**.

Assessment of material injectability

Injectability tests were performed by compressing a syringe piston loaded with the hydrogel solution using a traction/compression machine (model 2444, Instron, Norwood, MA, USA). The syringe (6 mL) was equipped with different needle sizes (18G, 20G, 22G and 24G, length: 3.8 cm), and pushed using a speed

of 2.5 mm/s, compatible with EN ISO 7886-1:2018. regulating the use of syringes. The force needed to allow material injection was recorded by the load cell of the instrument.

Assessment of nanocomposite hydrogel stability on the cartilage tissue

The stability of the hydrogels onto the cartilage tissue was assessed upon injecting the material solutions while varying the angle that the injector tip formed with respect to the cartilage tissue. The tissue was harvested from an adult bovine knee. A drop of ~20 µL was poured onto the cartilage, and a photo was taken after 2 s to assess its stability. Five trials were performed for each angle.

To evaluate the adhesion strength of the hydrogels to the cartilage tissue, a custom set-up was used, as reported in Trucco et al.[2] Cartilage samples from the knee of an adult bovine were cut using a surgical instrument for bone/cartilage biopsies (Longueur) with an inner diameter of 6.4 mm, and fit to the setup. Then, 400 µL of hydrogel were delivered onto the cartilage and left crosslinking. After hydrogel crosslinking, the hydrogel-hosting part was hooked to the load cell of the traction test machine, and the test was performed in traction modality (speed: 1 mm/min) until reaching the mechanical failure of the interface. Force curves as a function of the displacement were obtained from each test, and the adhesion strength (in kPa) was determined by dividing the force by the contact area between the hydrogel and the cartilage tissue. From each adhesion strength curve, the maximum adhesion strength value (in kPa) was obtained.

Controlled ultrasound stimulation

Two US systems, one for 38 kHz low-frequency stimulation and the other one for high-frequencies (1 MHz and 5 MHz) stimulation were used in this work (**Fig. 2a,b**). The detailed protocols are described in **Supplementary information, section S8.3**.

FEM simulations of the BTNP – US wave interaction

FEM analyses were carried out using COMSOL Multiphysics (V6.0), run on a MacBook Pro M1 Max ARM64 processor, with 64 GB RAM. The COMSOL “MEMS” and “Acoustics” modules were chosen to include the relevant physics of the acoustic pressure wave and the piezoelectric and dielectric response of the BTNP. The detailed methods are described in **Supplementary information, section S8.4**.

In vitro culture of human ASCs

ASCs were purchased from Lonza (Pharma&Biotech, Switzerland) (N=6) and were expanded by seeding 7,500 cells/cm^2 in T150 culture flasks and culturing them in α-MEM containing 5% isogrowth (IsoCellsGROWTH, Euroclone, Pero, IT) and 1% penicillin/streptomycin (Life Technologies) at 37°C in a 5% CO_2 incubator. Before encapsulation in the hydrogel, ASCs were phenotypically characterized for the CD markers CD31, CD34, CD45, CD73, CD90, CD105, CD166 as previously reported[3] and were analyzed for differentiation capability by using specific osteogenic and chondrogenic media as previously

described[4,5] to check that they satisfied the minimal criteria for defining multipotent mesenchymal stem cells[6].

ASCs encapsulated in the bare or nanocomposite hydrogel were cultured with chondrogenic medium (high-glucose DMEM supplemented with 50 mg/mL ITS + premix, 10^{-7} M dexamethasone, 50 µg/mL ascorbate–2phosphate, 1-mM sodium pyruvate, and 100 U/mL – 100 µg/mL penicillin–streptomycin, Sigma Aldrich) containing chondrogenic factors TGF-β3 (10 ng/mL) and BMP6 (10 ng/mL), both from Miltenyi Biotech, Auburn, CA, USA (**Extended data Fig. 5a**) or in inflammatory conditions (+ IL1β, 10 ng/mL) (R&D Systems, Inc., Minneapolis, MN, USA) (**Extended data Fig. 8c**). Cell culture medium was changed three times a week.

ASC-laden hydrogels treated with or without US (+ and -US) following specific experimental designs (**Extended data Fig. 5a, 6c, 7a, 7e, 8c**) were cultured for 2, 3, 10 and 28 days and evaluated for cell viability, cytotoxicity, and metabolic activity, gene expression, released factors, protein analysis and immunohistochemistry.

Viability of ASCs in the nanocomposite hydrogel

The viability of ASCs encapsulated in the nanocomposite hydrogel was evaluated by Live/Dead kit (Life Technologies). Samples were washed in D-PBS (Aurogene Srl, Rome, IT) and incubated with Live/Dead solution for 35 min at 37°C. Then, hydrogels were washed again with D-PBS and imaged, to discriminate live cells (in green) and the nuclei of dead cells (in red) with a fluorescence microscope (Nikon Instruments Europe BW). Quantitative analysis of stained slides was performed on five microscopic fields (×200 magnification) for each section. The analysis was performed using a Red/Green/Blue (RGB) tool within the Software NIS-Elements, at an Eclipse 90i microscope (Nikon Instruments Europe BV). The total number of green cells stained and the total number of positive-stained red cells were acquired. Data were expressed as a percentage of viable cells.

Cytotoxicity was assessed with a LDH assay kit (Roche, Mannheim, Germany). The supernatant was collected after 2 and 10 days and tested for the absorbance values at 490 nm by a microplate reader TECAN Infinite® 200 PRO (Tecan Italia S.r.l., Cernusco Sul Naviglio, Italy).

Cell metabolic activity was analyzed by Alamar Blue test. Briefly, the samples were incubated with 10% Alamar Blue (Life Technologies), and after 5 h, the absorbance was read at 570 and 600 nm using an automated spectrophotometric plate reader TECAN Infinite® 200 PRO (Tecan). The results were expressed as percentages of AlamarBlue reduction, as indicated by the manufacturer's data sheet (BioRad Laboratories).

For evaluating cell distribution within the hydrogels, the samples were fixed in 10% formaldehyde in D-PBS for 40 min, washed in D-PBS, dehydrated in ethanol, and embedded in paraffin. Thin sections (5 µm) were cut and stained for hematoxylin-eosin (Bioptica, Milan, Italy), then the slides were analyzed through a light microscope (Nikon Instruments Europe BW).

RNA isolation and quantitative PCR

Total RNA was extracted by treating all samples with 1 mL of Eurogold RnaPure (EuroClone S.p.a.). The samples were then immediately snap frozen in liquid nitrogen (-196 °C) and stored in a freezer at −80 °C. RNA extraction was performed by homogenizing samples and following the Eurogold manufacturer's instructions. The samples were then treated with DNase I (DNA-free Kit) and the RNA was quantified using a Nanodrop® spectrophotometer (EuroClone S.p.a). Reverse transcription was performed using Super Script® Vilo™ cDNA synthesis Kit (Life Technologies), according to the manufacturer's protocol.

qRT-PCR was performed by using TBGreen® Premix ExTaq™ (Takara Bio Inc. Shiga 525-0058, Japan) with LightCycler®2.0 (Roche Molecular Biochemicals). The gene markers quantified were: aggrecan (*ACAN*), collagen type 1 alpha 1 chain (*COL1A1*), collagen type 2 alpha 1 chain (*COL2A1*), collagen type 10 alpha 1 chain (*COL10A1*), the proliferation marker Ki-67 (*MKI67)*, matrix metalloproteinase 13 (*MMP13*), SRY-Box Transcription Factor 9 (*SOX9)* and Tissue inhibitor of metalloproteinase 1 (*TIMP1*) (see **Supplementary information, section S8.5**). The efficiency of all primers was confirmed as high (>90%) and comparable. For each target gene, Crossing Point (CP) values were calculated and normalized to the CP of the housekeeping reference gene Glyceraldehyde-3-Phosphate Dehydrogenase (*GAPDH)* according to the formula $2^{-\Delta Ct}$ and expressed as a percentage of the reference gene.

Immunohistochemistry and cytokine release measurements

On day 10 or 28, both hydrogel and nanocomposite treated with or without US were fixed in 10% formaldehyde in D-PBS for 40 min, washed in PBS, dehydrated in ethanol, and embedded in paraffin. Immunohistochemistry techniques were used to evaluate collagen type 2, proteoglycan and collagen type 1 expression. Serial sections of 5 µm were incubated for 60 min at RT with monoclonal mouse anti-human collagen type 2 (10 µg/mL), anti-human proteoglycan (5 µg/mL), anti-human collagen type 1 (5 µg/mL), all from Chemicon International, Temecula, CA, USA and polyclonal rabbit anti-human beta galactosidase (1 µg/mL) (from Proteintech Group, Rosemont, Illinois, USA), rinsed, and then sequentially incubated at RT for 20 min with multilinker biotinylated secondary antibody and alkaline phosphatase-conjugated streptavidin (Biocare Medical, Walnut CreeK, CA, USA). The colorimetric reactions were developed using fast red (Biocare Medical) counterstained with hematoxylin and mounted with glycerol jelly. The sections were evaluated with a bright field microscope (Nikon Instruments Europe BW). Negative and isotype-matched control sections were performed.

Apoptotic cells were detected using the In Situ Cell Death Detection Kit, AP (Merck, Darmstadt, Germany), following the manufacturer's instructions. Semiquantitative analyses on the stained slides were performed by acquiring 20 microscopic fields (×200 magnification) for each section. The analysis was performed using RGB with the software NIS-Elements and using an Eclipse 90i microscope (Nikon Instruments Europe BV). Briefly, we acquired the total number of blue-stained nuclei and the total number of positive-stained red cells and data were expressed as a percentage of positive cells.

The analysis of IL6 and IL8 release in the supernatant was purused using multiplex bead-based sandwich immunoassay kits (BioRad Laboratories Inc., Segrate, Italy) following the manufacturer's instructions.

Proteomic analysis, liquid chromatography-Tandem mass spectrometry (LC-MS/MS) and bioinformatic analysis

The total proteins were extracted and analyzed to assess the differential protein expression between the samples (nanocomposite with and without the application of US). The detailed protocols for sample treatment, data collection and analyses are reported in **Supplementary information, section S8.6**.

In vitro genotoxicity tests and *in vivo* biocompatibility tests

In vitro genotoxicity tests were performed by following ISO 10993-3:2015 (Biological evaluation of medical devices - Part 3: Tests for genotoxicity, carcinogenicity and reproductive toxicity) by applying the Ames and micronuclei tests. The Ames bacterial reverse mutation assay (Ames MPF™ Penta II kit, Xenometrix AG, Switzerland), was performed on four *Salmonella typhimurium* strains and one *Escherichia coli* strain, evaluating revertant colonies after a 90 min exposure to the nanocomposite hydrogel and a 48 h culture period. The cell micronuclei assay was performed on human lymphoblastoid TK6 cell line (ATCC, lot 59429029), for 3 and 24 h exposure periods, after which the relative population doubling (RPD) and the micronuclei frequencies were assessed.

All *in vivo* procedures were conducted strictly following the Italian Law on animals used for scientific purposes (Decree n. 26/2014): the project was authorized by the Italian Ministry of Health (n. 777/2021-PR) on the 3rd November 2021. Skin irritation tests were carried out following ISO 10993-23 (2021) on New Zealand SPF white male rabbits. Nanocomposite hydrogel, negative control and a positive known sensitizer were topically applied on the shaved dorsum region. After 4 h exposure, the treated sites were scored for erythema and oedema at 1, 24, 48 and 72 h. The Primary Irritation Index (PII) (minimum 0-maximum 8) was calculated according to the ISO 10993-23 standard. Acute systemic toxicity tests were carried out following ISO 10993-11 (2018) by single dose intramuscular nanocomposite injections on Sprague Dawley male rats. Clinical observations, signs of illness, pain, injury at the main apparatuses and systems, any behavioral alteration, and weight, water and food intake measurements were registered at baseline and at 24, 48, 72 h after treatment. Delayed type hypersensitivity tests were carried out following ISO 10993-10 (2010) on Dunkin Hartley guinea pigs, scoring erythema and oedema by Magnusson and Kligman grading scale after 24 h and 48 h[7]. The detailed protocols are reported in **Supplementary information, section S8.7**.

Statistical analyses

All data were analyzed using GraphPad Prism version 9.0.0 for Windows (GraphPad Software, San Diego, California USA, www.graphpad.com). D'Agostino-Pearson Normality test was performed on all data; data showing a normal distribution were analzyed using parametric tests, while data . data showing a non-normal distribution were analzyed using non-parametric tests.

Experimental data concerning DNA, LDH, metabolic analyses, DLS measurements, rheological indexes (K and n), estimated shear stress to the cells (using different needles), degradation rate, injection force, adhesion strength and COF were analyzed by applying a non-parametric Kruskal–Wallis test and Dunn's multiple comparison test to analyze significant differences between groups.

Data concerning compressive modulus, swelling ratio and sol-gel fraction were analyzed by applying a non-parametric Mann-Whitney U-test to compare non-doped and doped hydrogels.

Experimental data derived from *in vitro* tests on ASCs were analyzed by applying a Mann-Whitney test or Wilcoxon test or Kruskal–Wallis one-way ANOVA and Dunn's multiple comparison tests or Friedman and Dunn's multiple comparison tests to analyze significant differences between groups.

Data from *in vitro* genotoxicity and *in vivo* biocompatibility tests were analyzed by applying a Shapiro-Wilk test and a Student's t test when comparison versus CTR- was needed; otherwise, a two-way ANOVA followed by Sidak's multiple comparison test was conducted.

For all tests, the significance threshold was set at $p<0.05$.

Sample size, randomization and blinding

For *in vitro* tests, the sample size was chosen based on previous laboratory experience considering a minimum of at least two independent experiments and a triplicate of independent samples. For genotoxicity and *in vivo* tests, the sample size was established based on the OECD guidelines and UNI EN ISO 10993 standard, which define the minimum number of samples/animals per group and test and guarantee the statistical validity of the results. No method of randomization was followed and no animals were excluded from this study. For *in vitro* tests, investigators were not blinded to sample allocation during the experiments and assessment of results. For *in vivo* tests, caregivers and the veterinary doctor were not blinded, whereas outcome assessors were blinded to the subject's allocation.

Fig. 1. In **c**, the image is representative of five independent experiments; in **f, g, h** and **i**, n = 5 per group.

Fig. 3. In **b**, the images are representative of ten independent experiments; in **c**, the images are representative of six independent experiments, n=6 per group; in **d**, n=4 per group; in **e**, n=16 per group; in **f**, the images are representative of three independent experiments, n=12 per group; in **g**, the images are representative of five independent experiments, n=20 per group; in **h**, six independent experiments, n=18 per group; in **i**, six independent experiments, n=12 per group.

Fig. 4. In **a**, the image is representative of two independent experiments; in **b**, the image is representative of two independent experiments; in **c**, two independent experiments, n=10 per group; in **d**, two independent experiments, n=5 per group; in **e**, two independent experiments, n=5 per group; in **f**, two independent experiments, n=7 per group, the images are representative of two independent experiments; in **g**, duplicate cultures were performed for testing negative and positive controls and three different concentrations of the test substance. Micronuclei were scored on 2,000 cells, equally divided among the

two replicates, for each tested condition; in **h**, healthy young adult New Zealand SPF white male rabbits were used for testing the nanocomposite hydrogel and negative control (n=3) and for positive control (n=1); in **i**, healthy Sprague Dawley male rats were used for testing the nanocomposite hydrogel and negative control (n=5 per group); in **j**, healthy Dunkin Hartley male and female guinea pigs were used for testing negative control (n=5), positive controls (n=10) and nanocomposite hydrogel (n=10).

Extended data Fig. 1. In **a**, the image is representative of five independent experiments; in **b**, three independent experiments; in **c**, five independent experiments per group (particle and background); in **e**, images are representative of two independent experiments; in **f**, n=6 per group; in **g**, n=2, images are representative of five images per sample analyzed; in **h**, n=3 per group; in **i** and **j**, n=4 per group.

Extended data Fig. 2. In **b**, images are representative of two independent experiments; in **c**, n=6 per group; in **e**, n=2, images are representative of five images per sample analyzed; in **f**, n=3 per group; in **g** and **h**, n=4 per group.

Extended data Fig. 3. In **b**, FT-IR graphs are representative of two independent experiments; in **c**, **d**, **e**, **f**, **g**, and **h**, n = 5 per group; in **j**, n = 5 per each angle tested; in **k** and **j**, n = 5 per group.

Extended data Fig. 5. In **b**, the images are representative of ten independent experiments; in **c**, the images are representative of six independent experiments, n=6 per group; in **d**, n=4 per group; in **e**, n=16 per group; in **f**, the images are representative of three independent experiments, n=12 per group; in **g**, the images are representative of five independent experiments, n=20 per group; in **h**, 6 independent experiments, n=18 per group; in **i**, six independent experiments, n=12 per group.

Extended data Fig. 6. In **a**, the image is representative of three independent experiments; in **b**, n=3 per group; in **d**, images are representative of two independent experiments; in **e**, the image is representative of two independent experiments.

Extended data Fig. 7. In **b**, the image is representative of three independent experiments; in **c**, **d**, **e**, **f** and **g**, two independent experiments, n=4 per group.

Extended data Fig. 8. In **a** and **b**, data refer to two independent experiments.

Extended data Fig. 9. In **a**, the Ames experiment was performed on five different bacterial strains, n=3 for each material and each concentration tested; in **c**, Micronuclei experiments were run in duplicates.

Data availability

The datasets generated and analyzed during the current study are available from the corresponding author on reasonable request. Mass spectrometry and proteomics data have been deposited to the ProteomeXchange Consortium via the PRIDE[8] partner repository with the dataset identifier PXD038147 and 10.6019/PXD038147. Username: reviewer_pxd038147@ebi.ac.uk. Password: PipAjUfZ.

Code availability

The code of the COMSOL routine used for FEM simulations of nanoparticles-US waves interactions is available in **Supplementary Data File 1**.

Methods References

1. Vannozzi, L. et al. Graphene oxide and reduced graphene oxide nanoflakes coated with glycol chitosan, propylene glycol alginate, and polydopamine: characterization and cytotoxicity in human chondrocytes. *Nanomaterials* **11**, 2105 (2021).
2. Trucco, D. et al. Primers for the adhesion of gellan gum-based hydrogels to the cartilage: a comparative study. *Macromol. Biosci.* **22**, 2200096 (2022).
3. Manferdini, C. et al. RGD-functionalized hydrogel supports the chondrogenic commitment of adipose mesenchymal stromal cells. *Gels* **8**, 382 (2022).
4. Manferdini, C. et al. Chitosan-based scaffold counteracts hypertrophic and fibrotic markers in chondrogenic differentiated mesenchymal stromal cells. *J. Tissue Eng. Reg. Med.* **13**, 1896-1911 (2019).
5. Maumus, M. et al. Adipose mesenchymal stem cells protect chondrocytes from degeneration associated with osteoarthritis. *Stem Cell Res.* **11**, 834-844 (2013).
6. Dominici, M.L.B.K. et al. Minimal criteria for defining multipotent mesenchymal stromal cells. The International Society for Cellular Therapy position statement. *Cytotherapy* **8**, 315-317 (2006).
7. Magnusson, B., & Kligman, A.M. The identification of contact allergens by animal assay. The guinea pig maximization test. *J. Invest. Dermatol.* **52**, 268-276 (1969).
8. Perez-Riverol Y et al. The PRIDE database resources in 2022: A Hub for mass spectrometry-based proteomics evidences. Nucleic Acids Res. **50**, D543-D552 (2022).

Declarations

Acknowledgments

This work received funding from the European Union's Horizon 2020 research and innovation program, grant agreement No 814413, project ADMAIORA (ADvanced nanocomposite MAterIals fOr in situ treatment and ultRAsound-mediated management of osteoarthritis). The authors acknowledge the contribution of Laura Riacci and Lorenzo Arrico for their technical support during nanocomposite preparation and testing, Liliana Agresti for her technical support during nanomaterial cytotoxicity assessment, Mariana Oliveira for her technical support during material adhesion strength assessment, Nadeshda Severina for her technical support during barium titanate nanoparticle synthesis and characterization, Pasqualantonio Pingue for his support during PFM data acquisition, Katia Samoggia, Luca Fergnani, Daniel Fota, Salvatore Pellini and Umberto Bonanno for their technical support in the activities at Complex Structure Surgical Sciences and Technologies.

Author contributions

L.R., A.C., C.M., D.T., L.V., M.Ts. and G.L. planned and designed the main experiments, elaborated and interpreted the results. M.G. and P.P. performed TEM and EDX analyses. Y.F. and C.J. planned and performed the synthesis and BET/DLS characterization of BTNPs. G.D.N, E.T. and M.Te. planned and performed the synthesis and characterization of GO nanoflakes. A.C., F.F., E.D. and L.R. conceived and developed the set-up design for controlled *in vitro* ultrasound stimulation. M.C. and A.C. developed the analytical and numerical models of the interaction between BTNPs and ultrasound. L.V. and D.T. performed nanomaterial coating, hydrogel preparation, assessment of nanomaterial stability and characterization of the nanocomposite hydrogels. L.V. performed *in vitro* assessment of BTNPs and GO cytocompatibility on human chondrocytes and performed piezoelectric force microscopy analyses on BTNPs. D.T. was enrolled in the sample management for *in vitro* experiments on ASCs and in the material preparation for *in vivo* experiments. C.M., G.L., M.F. planned and designed the *in vitro* experiments. C.M., E.G., P.D., Y.S., E.L. performed *in vitro* viability and chondrogenic assays and collected and elaborated data. M.C. performed electron microscopy analyses. M.P. and J.B. performed proteomic analysis and data elaboration. M.Ts., L.M., M.F. were involved in obtaining ethical authorizations for *in vivo* tests. M.Ts. planned *in vivo* tests. M.Ts., C.D., G.C. and L.M. performed *in vitro* and *in vivo* biocompatibility tests and data analysis. A.A. interpreted experimental data and elaborated them to create the paper figures and videos. L.R. wrote the manuscript with input from all authors. These authors contributed equally: A.C., C.M., D.T. and L.V.

Competing interest declaration

The authors declare no competing interests.

Figures

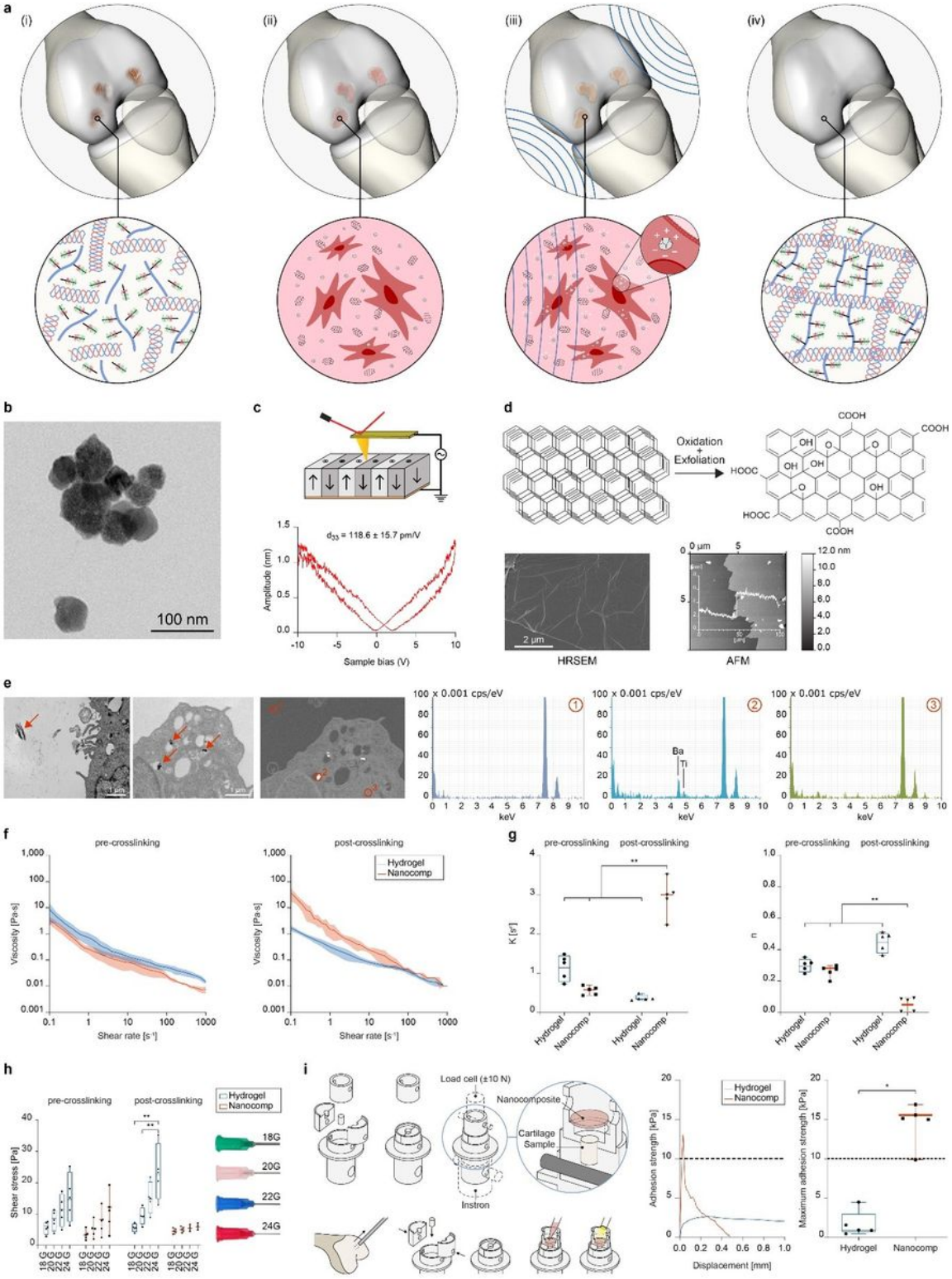

Figure 1

Nanocomposite hydrogel embedding BTNPs, GO nanoflakes and human ASCs. a, Depiction of the target therapeutic paradigm: *(i)* degenerated cartilage tissue, *(ii)* application of the cell-laden nanocomposite hydrogel *in situ*, *(iii)* stimulation with US waves, *(iv)* regenerated cartilage tissue. **b**, TEM image of BTNPs. **c**, Depiction of PFM, used to assess BTNP piezoelectric properties (top) and graph showing BTNP ferroelectric behavior, with the d_{33} coefficient (bottom). **d**, Process used to obtain GO nanoflakes from

graphene (top) and representative results of HR-SEM and AFM analyses (bottom). **e**, TEM images showing clusters of BTNPs internalized in cell vacuoles, and GO nanoflakes outside the cells (left) and EDX spectra (right). **f**, Viscosity *vs* shear rate plots. **g**, K and n indexes extracted by viscosity *vs* shear rate curves. **h**, Estimated shear stress acting on cells for different needles (18G, 20G, 22G, 24G). **i**, (left-top): depiction of the set-up used to evaluate the adhesion strength *ex vivo*; (left-bottom): procedure for performing the test; (right): representative stress-strain curves and maximum adhesion strength data. In b,f, data are represented as mean ± s.d. In g,h,i, data are represented as box plots with median, minimum and maximum. *p<0.05, **p<0.01.

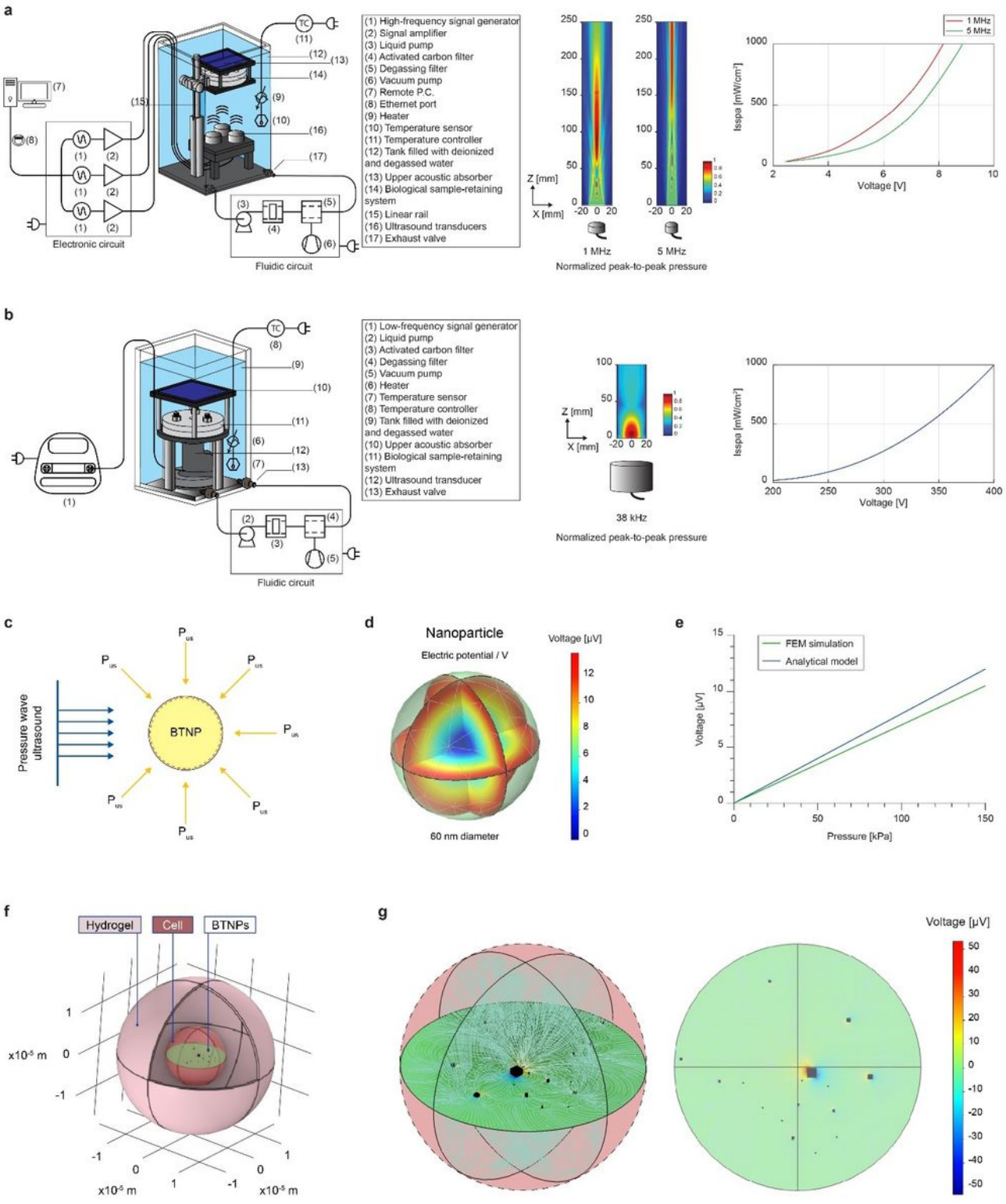

Figure 2

Set-up for dose-controlled US stimulation and modeling of nanocomposite-US wave interaction. a, Components of the high-frequency US stimulation system adopted in the study (left), normalized peak-to-peak pressure field maps (center), and spatial-average pulse-average intensity measurements results as a function of the input voltage provided by the generator at 1 and 5 MHz (right). **b**, Components of the low-frequency US stimulation system adopted in the study (left), normalized peak-to-peak pressure field map

(center), and spatial-average pulse-average intensity measurements result as a function of the input voltage provided by the generator at 38 kHz (right). **c**, Scheme of a single BTNP invested by a plane pressure wave expressed as hydrostatic pressure. **d**, Visualization of the electric potential developed by a single BTNP invested by a peak-to-peak hydrostatic pressure of 172 kPa, corresponding to a spatial average pulse average intensity of 250 mW/cm^2. **e**, Maximum voltage generated by a single BTNP as a function of the hydrostatic pressure: comparison between the analytical model and the FEM simulations. **f**, Scheme of the 3D COMSOL framework. **g**, Electric potential in a representative 2D plane in which BTNPs are located ($P_{pk\text{-}pk}$=172 kPa).

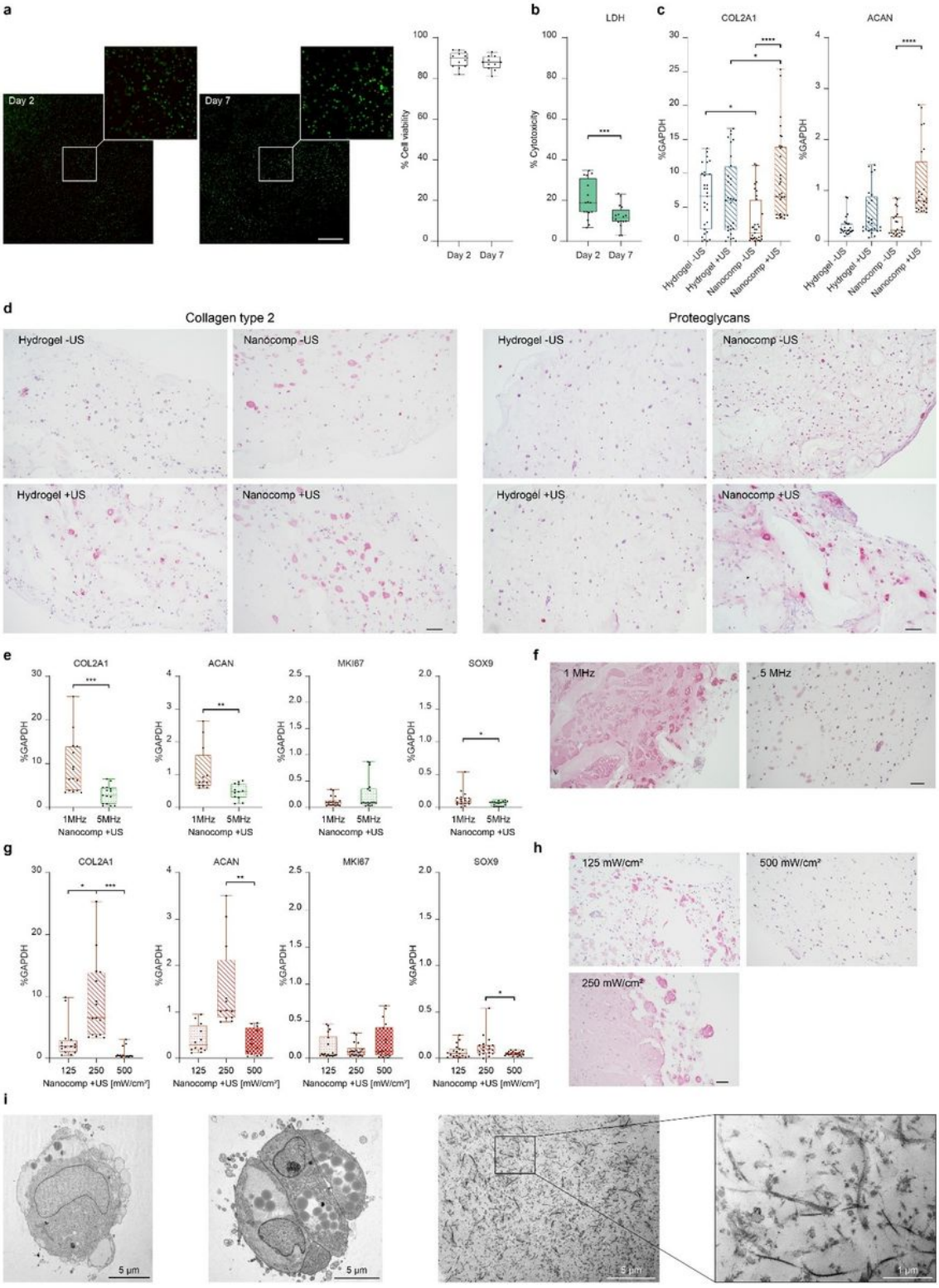

Figure 3

Viability and US-induced chondrogenesis of ASCs embedded in the hydrogels. a, Live/Dead assay performed on ASCs encapsulated in the nanocomposite hydrogel on day 2 and 7. Viable cells are shown in green; dead cells are shown in red. Scale bar = 500 µm. The graph shows the quantification of viable cells. **b**, LDH release from ASCs embedded in the nanocomposite hydrogel on day 2 and 7. Data are expressed as a percentage of cytotoxicity. **c**, Expression of *COL2A1* and *ACAN* genes on day 10 in

Hydrogel and Nanocomp, with and without US stimulation. Data are expressed as a percentage of the *GAPDH* housekeeping gene. **d,** Collagen type 2 (left) and proteoglycans (right) immunostaining on day 10 in Hydrogel and Nanocomp, – and + US. Scale bars = 100 µm. **e**, Expression of *COL2A1*, *ACAN*, *SOX9* and *MKI67* genes on day 10. **f**, collagen type 2 immunostaining on day 28 corresponding to different US frequencies. Scale bar = 100 µm. **g**, Expression of *COL2A1*, *ACAN, MKI67* and *SOX9* genes on day 10. **h**, collagen type 2 immunostaining on day 28 corresponding to different US intensities. **i**, Representative TEM images (on day 28) of Nanocomp + US samples stimulated at 1 MHz and 250 mW/cm^2. In a,b,c,e,g, data are represented with box plots showing the median, minimum, and maximum values. *p<0.05, **p<0.01, ***p<0.001, ****p<0.0001.

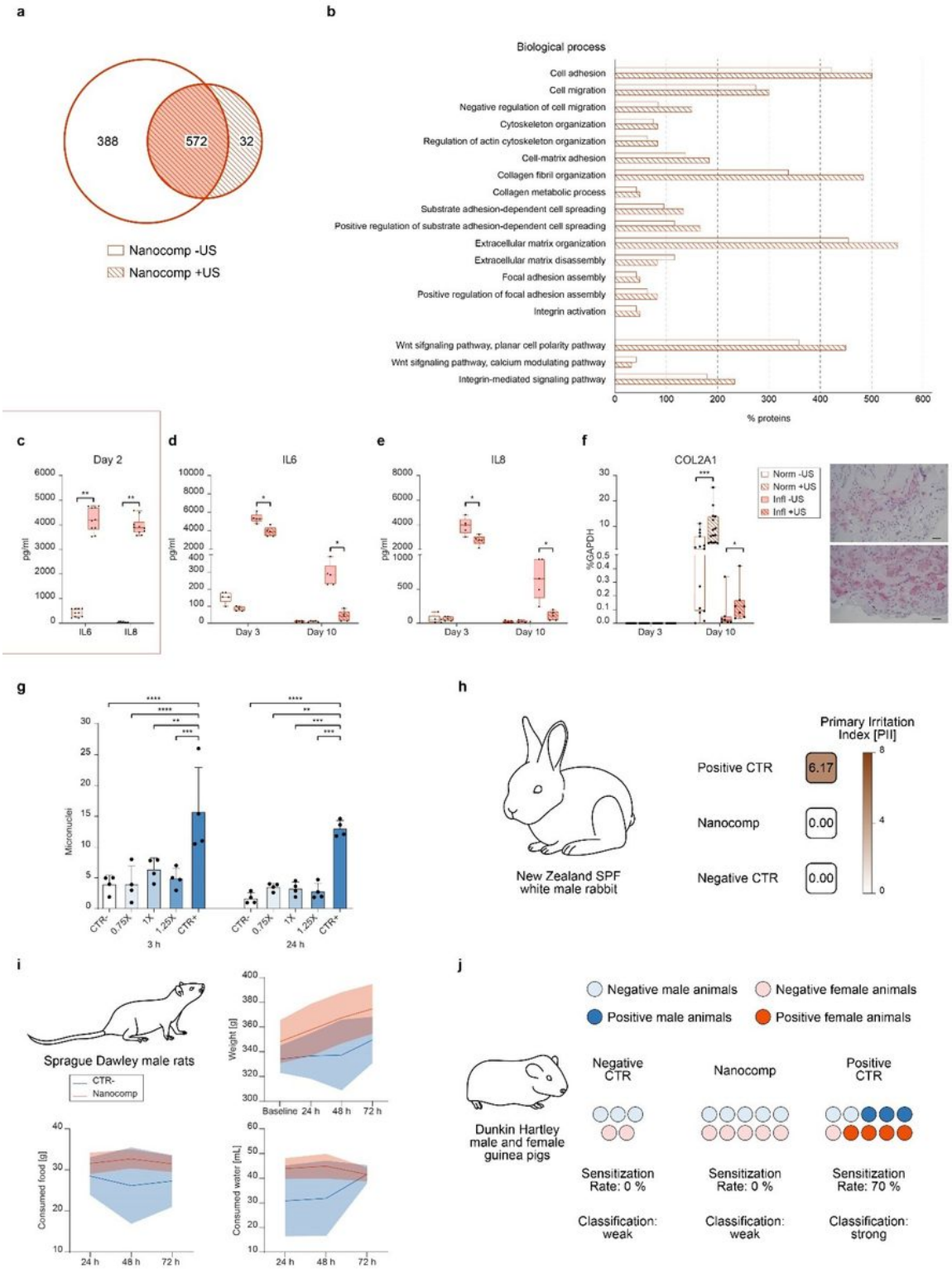

Figure 4

Mechanisms underlying the US-piezoelectric nanomaterial effects, *in vitro* genotoxicity and *in vivo* safety of the nanocomposite hydrogel. a, Venn diagram (left) showing the proteins identified by LC-MS analysis. **b**, Bars represent % of proteins belonging to Gene Ontology biological terms comparing the Nanocomp - US and the Nanocomp + US datasets. **c**, IL6 and IL8 release on day 2. **d**, IL6 release on day 3 and day 10. **e**, IL8 release on day 3 and day 10. **f**, COL2A1 gene expression on day 3 and day 10.In **c-f**, analyses were

conducted in Norm and Infl – and +US samples. Collagen type 2 immunostaining on day 28 in Infl – and + US samples. In c-f, data are represented with box plots showing the median, minimum, and maximum values. **g**, Results of the *in vitro* genotoxicity test: micronuclei frequencies after exposing TK6 cells to three different concentrations of Nanocomp, negative (CTR-, no treatment) and positive (CTR+, 0.5 mg/mL H_2O_2) controls for 3 and 24 h. Data are reported as mean ± SD . **h**, Results of primary irritation indexes obtained in skin irritation tests carried out in rabbits treated by topically applying the Nanocomp or a saline solution (CTR-) or a known irritant (CTR+). **i**, Results of the acute systemic toxicity test carried out in rats treated with intra muscular injections of Nanocomp, or saline solution (CTR-). **j**, Results of the delayed type-hypersensitivity test performed in male and female guinea pigs. *p<0.05, **p<0.01, ***p<0.0010, ****p<0.0001.

Supplementary Files

This is a list of supplementary files associated with this preprint. Click to download.

- NatureSupplementaryInformation.docx
- Supplementaryvideo4.mp4
- Supplementaryvideo2.mp4
- Supplementaryvideo1.mp4
- Supplementaryvideo3.mp4
- ExtendedDataFigs.docx